

# Inkjet Printing on Hydrophobic Surface: Practical Implementation of Stacked Coin Strategy

Matthew J. Docherty, Paria Naderi, Gerd Grau, Khellil Sefiane, and Alidad Amirfazli\*

While inkjet printing on many hydrophilic surfaces is achieved through control of drop spacing and droplet deposition delay, the same for hydrophobic substrates proves challenging. Low surface energies of hydrophobic surfaces prevents intact and uniform lines of low-viscosity ink to form. In this article, the stacked coin printing strategy used for hydrophilic surfaces, is adapted for hydrophobic surfaces. Stacked coin morphology is seen when droplet deposition time between two sequentially deposited droplets is longer than the evaporation time of the first droplet. On hydrophobic surfaces, the parameter window for successful printing is smaller than on hydrophilic surfaces, thus an investigation is needed to implement this methodology. Experiments were conducted using an inkjet printer with variable stage speed and stage temperature. Silver nanoparticle ink was used to print on Teflon-AF substrates. We identified the following regimes: isolated droplets, isolated multi-droplets, broken line, true stacked coin, and delamination. The relationship between substrate temperature, drop spacing, and droplet deposition delay controls the occurrence of each regime. In this study, 180 °C was identified as the critical temperature for instantaneous drying of the studied ink, and a maximum drop spacing of 20 μm to print continuous lines.

## 1. Introduction

In recent decades, there have been widespread advancements and research into mass-producing electronics. Non-contact printing methods, like inkjet printing, do not require a master for the printing of specific patterns, allowing the user to print specific patterns of low-viscosity ink on demand. Additionally, the procedure of inkjet printing electronics has acquired widespread attention for its cost benefits and eco-friendlier manufacturing, while producing well-defined patterns on hydrophilic surfaces.<sup>[1–3]</sup> Inkjet printing has allowed patterns to be printed on a variety of surfaces ranging from paper to Teflon-amorphous fluoropolymer (AF) with plasma pretreatment.<sup>[4,5]</sup> While the printability and ink behavior have been well documented for hydrophilic surfaces allowing users to achieve uniform connected lines, the characteristic low surface energy of hydrophobic substrates creates significant challenges for printing, especially for non-contact printing

techniques, e.g., inkjet printing.

Attempting to print lines on hydrophobic surfaces results in droplets coalescing together and forming bulges of liquid and thus dewetting the surface. This phenomenon prevents the production of uniform connecting lines on hydrophobic surfaces when attempting the same techniques that are used for hydrophilic surfaces.<sup>[6]</sup> For the inkjet printer to retain its characteristic adaptability for use in mass production, techniques must be readily available to print on both hydrophobic and hydrophilic substrates. Surfaces such as polytetrafluoroethylene (PTFE) are advantageous for their low friction coefficient, chemical inertness, and thermal stability, making them desirable in the manufacture of a variety of specialty products, e.g., biomedical devices.<sup>[7,8]</sup> Additionally, fluoropolymers are ideal materials for use as the gate dielectric in organic thin-film transistors (OTFTs) often printed with silver nanoparticle inks, or similar.<sup>[5,9–12]</sup> Fluoropolymers are advantageous due to their low dielectric constants enhancing charge transport,<sup>[9]</sup> and characteristic water repellence, which also acts as encapsulation and prevents doping.<sup>[12,13]</sup> Plasma/UV treatment of hydrophobic surfaces is one of the most common methods to enable printing on such substrates by rendering them hydrophilic, with many studies using this technique to develop and study printing on hydrophobic substrates.<sup>[7,14–17]</sup> Other methods exist to enable printing on hydrophobic surfaces, such as physical manipulation of the

M. J. Docherty, K. Sefiane  
School of Engineering  
The University of Edinburgh  
Edinburgh EH9 3FD, Scotland, United Kingdom of Great Britain and Northern Ireland

M. J. Docherty, A. Amirfazli  
Department of Mechanical Engineering  
York University  
Toronto, Ontario M3J 2S5, Canada  
E-mail: alidad2@yorku.ca

P. Naderi, G. Grau  
Department of Electrical Engineering and Computer Science  
York University  
Toronto, Ontario M3J 2S5, Canada

 The ORCID identification number(s) for the author(s) of this article can be found under <https://doi.org/10.1002/adem.202400237>.

© 2024 The Authors. Advanced Engineering Materials published by Wiley-VCH GmbH. This is an open access article under the terms of the Creative Commons Attribution-NonCommercial-NoDerivs License, which permits use and distribution in any medium, provided the original work is properly cited, the use is non-commercial and no modifications or adaptations are made.

DOI: 10.1002/adem.202400237

substrate surface through the implementation of a surface level cube lattice structure, using photolithography,<sup>[18]</sup> the addition of an intermediate hydrophilic polymer layer,<sup>[19,20]</sup> and the employment of soft lithography to produce wettability patterns on the surface of the substrate. However, the aforementioned methods all involve the use of time-consuming pretreatment or/and post-treatment of the substrate used for printing.<sup>[7,14,15,19,21]</sup>

Here, a method to overcome the difficulties of printing on hydrophobic substrates through stage heating has been developed. The method is an adaptation of stacked coin printing, a technique, which has been successful in the production of conductive lines on hydrophilic surfaces for, e.g., thin-film transistors<sup>[22]</sup> and conductive films.<sup>[23]</sup> Stacked coin printing is a technique in which the time taken to deposit a subsequent overlapping droplet in a pattern is longer than the evaporation time of the prior droplet.<sup>[3]</sup>

Conductive inks composed of nanoparticles (e.g., silver, gold, copper, etc.),<sup>[8,24]</sup> a solvent, and potentially other additives are the workhorse of the printed electronics industry. When dried, due to the silver content, the ink becomes hydrophilic. Taking advantage of the hydrophilic nature, we have shown previously that wet ink can be anchored to a dried ink spot.<sup>[6]</sup> The effect of impacting droplets experiencing a wettability gradient between the low surface energy substrate and the hydrophilic attraction to the previously dried hydrophilic droplet prevents the normal application of the stacked coin technique. The drying time of the droplet under room-temperature conditions supersedes the time taken for a wet droplet to completely dewet from its initial impact position and completely overlap the previous dried droplet in the system. Through manipulation of this situation, by accelerating the rate of drying of ink through stage heating, we can adapt the stacked coin method for use on hydrophobic surfaces. This work has defined the window for successful printability relating key parameters of droplet spacing, stage temperature, and print stage movement speed.

## 2. Experimental Section

A custom-built inkjet printer was used that provided stage movement in the  $x$ ,  $y$ , and rotational axes with an accuracy of  $1\ \mu\text{m}$ . The printer setup consisted of an ink reservoir and tube, nozzles, a pressure control unit, an actuator circuit, and the interface software, represented in **Figure 1**. The heated printer chuck is moved by individual motorized linear stages to allow full vector printing and the computer interface was developed through Lab View. The stage was programmed to come to a complete stop to jet the droplet before moving to the subsequent position; this meant that the stage has a speed limit based on both drop spacing and the maximum stage acceleration of  $256\ 000\ \mu\text{m}\ \text{s}^{-2}$ . The printer was operated in a drop-on-demand (DOD) mode with a Microfab  $60\ \mu\text{m}$  orifice nozzle (MJ-ATP-01-60-8MX, Microfab Technologies, Inc. Plano, TX), controlling precise droplet ejection through a piezoelectric transducer. The specific piezoelectric waveform was  $0\ \text{V}$  idle voltage,  $28\ \text{V}$  dwell voltage,  $-28\ \text{V}$  echo voltage, dwell time of  $30\ \mu\text{s}$ , echo dwell time of  $60\ \mu\text{s}$ , an initial rise and fall time of  $8\ \mu\text{s}$ , and a secondary rise time of  $5\ \mu\text{s}$ . Droplets are approximately  $0.2\ \text{nL}$  at ejection. We did not study the effect of ink droplet impact velocity onto the surface; this decision was made in the light of many available correlations that describe the relationship between drop impact velocity (or by proxy Weber number) and maximum spreading of the droplet upon impact, e.g., see refs. [25,26]. Note that the maximum spreading will determine primarily the width of the printed lines, and an estimate can be calculated readily using any of the correlations stated earlier. As such, we focused the work on unexplored parameters. A silver nanoparticle ink (Anapro, DGP 40LT-15C) was used for experimentation; it had 30%–35% by weight nanoparticle silver suspended in triethylene glycol monoethyl ether solvent. With the surface tension, viscosity, and density of the ink being  $34.65\ \text{mN}\ \text{m}^{-1}$ ,  $13.7\ \text{cP}$ , and

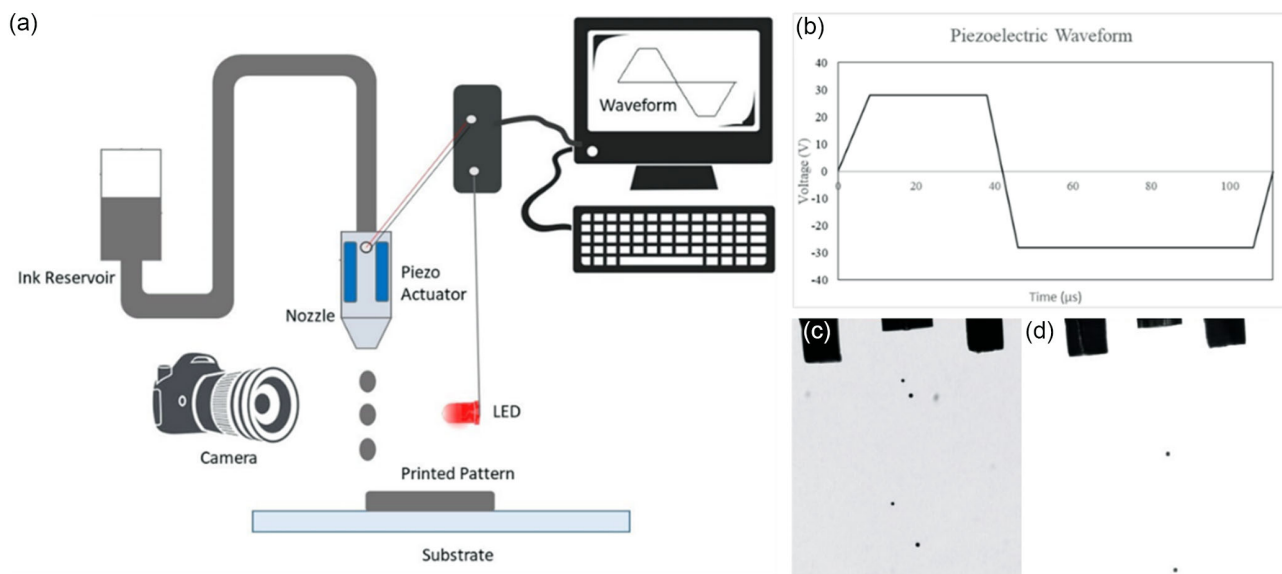


**Figure 1.** a) Schematic representation of custom-built printer setup. b) Piezoelectric waveform used to produce stable stream of droplets on ejection. c) Example of unstable satellite droplet formation, unsuitable for printing. d) Pictorial evidence of stable droplet stream achieved through actuation of waveform (b).

1450 kg m<sup>-3</sup>, respectively, based on these properties, the ink falls inside the printability range for inkjet printing.<sup>[27,28]</sup> The Z number is used to understand the influence of viscosity on droplet formation, a high Z number indicate high inertia within the droplets, increasing the likelihood of satellites on the liquid jet, while a lower Z number contributes toward more stable jetting. Thus, through controlling the Z number and manipulation of the piezoelectric waveform, we were able to achieve stable droplet jetting.<sup>[27,28]</sup> The nozzle was held at z distances from the stage of 1–2 cm to prevent nozzle clogging and ensure jetting remained consistent between experiments. Printing only began once stable droplet jetting was achieved in the absence of satellite droplets, verified through the use of a camera and a strobe light emitting diode (Figure 1a,c).

The substrate used was Teflon-AF 1600 (Sigma-Aldrich, Oakville, Canada) coated on glass microscope slides. Coating of microscope glass slides was achieved through spin coating at 500 rpm for 60 s. Teflon-AF solution was allowed to dry at 150 °C for 30 min before being translated over to the printer. The contact angle of the ink on the substrate surface was measured to be 84°. Despite the ink contact angle being <90°, the system still exhibits significant hydrophobic tendencies; thus, the system is considered hydrophobic (note: the hydrophobicity of a surface is measured and defined against water; Teflon-AF has a stable water contact angle of 113°).<sup>[29]</sup>

The independent variables used in this investigation were substrate/stage temperature (150–180 °C), the drop spacing (5–30 μm), and the stage movement speed. Due to the limitations of stage acceleration and the small drop spacings necessary to achieve stacked coins on hydrophobic substrates, the maximum average speed is limited differently for each drop spacing investigated, highlighted in **Table 1**.

The high values of temperature adopted here are due to the hydrophobic nature of the substrate, since the drying time of impacting droplets is a crucial factor to consider for the success of this proposed method. Temperatures surrounding the recommended sintering temperature of the ink quoted by the manufacturer were initially investigated and proved as an optimal starting point for investigation. Stage movement speed was varied from 5 μm s<sup>-1</sup> to the maximum speed that can be achieved, limited by stage acceleration for the specific drop spacing investigated (see Results section for specific values). On a fundamental level, these three variables (stage temperature, printing speed, and drop spacing) have been proven to affect printed line morphology in tandem, being the main three effective factors that can directly be controlled by the printer. The Experimental Section is outlined in **Figure 2**.

Upon nozzle clogging, the nozzle was forward flushed with iso-propanol (IPA) in a sonication chamber, then backflushed with IPA heated to 80 °C. Substrate roughness, ink concentration, and atmospheric pressure were assumed constant throughout printing. Additionally, it is assumed that the substrate can be

considered flat, with optical profilometry data showing minimal variances in the order of 10–100 nm as seen in **Figure 3f**.

Experiments were conducted at standard atmospheric and room-temperature conditions. To ensure reliability, experimental runs were performed 2–5 times producing lines 1 mm in length.

### 3. Results and Discussion

The applicability of the proposed method is discussed here by attempting to print straight lines. The printed lines can be categorized into several uniquely identified regimes. The identified regimes are isolated droplets, isolated multi-droplets, broken line, true stacked coin, and delamination. Examples of the morphologies present within each of these regimes can be seen in **Figure 3**. Through the observation of dried ink patterns, the mechanisms that yield specific ink morphologies can be identified. These mechanisms indicate distinct changes in printability, which reflect the onset of successful line formation. Through observation and categorization of the governing mechanisms of line formation, ink behavior at specific experimental conditions was characterized into the aforementioned regimes. Analysis of specific mechanisms leading to ink behaviors is discussed further later.

Each independent variable is investigated to determine a corresponding limiting condition, e.g., instantaneous drying temperature, maximum achievable drop spacing, and onset of asymmetric droplet spreading, all of which will be expanded upon later.

The isolated droplet regime is largely a temperature-dependent regime (**Figure 3a**). This regime occurs when the drying time of the droplets is substantially longer than the dewetting time and the droplet deposition interval (note: deposition interval for isolated droplet regime has been observed between 0.167 and 8.7 droplets s<sup>-1</sup>, determined via average stage velocity and drop spacing). Overlapping wet droplets on the surface do not dry sufficiently quickly to prevent them from completely dewetting from the surface and so merging with the previously deposited droplet. If two successive droplets are wet, then they merge due to energy minimization. If one droplet is dry but the newly deposited drop does not dry quickly, the wettability gradient caused by the hydrophilic dry droplet and the hydrophobic substrate causes merging. This regime leaves large, isolated droplet profiles at regular intervals which is akin to the expected result when printing lines on hydrophobic surfaces at room temperature. The temperature of the surface has not yet reached a state in which it can affect line morphology. This regime is similar to the isolated droplet regime defined in ref. [3]. However, this regime differs as the isolated droplet profiles on hydrophobic surfaces are made up of multiple droplets and are characteristic of dewetting, unlike isolated droplet regimes identified for hydrophilic surfaces made of single drops.<sup>[3]</sup> In this study, the isolated droplet regime was seen for any drop spacings greater than 70 μm.

The isolated multi-droplet regime (**Figure 3b**) is comparable to that of the isolated droplet regime; however, the morphology of droplet groups begins to take a more ovalar shape as regularly occurring groups of droplets can be observed, showing the onset of an instantaneous drying condition. The instantaneous drying condition can be defined as the temperature at which the surface

**Table 1.** Maximum average stage speed at each investigated drop spacing.

Drop spacing [μm]	5	10	15	20	25	30
Maximum average stage speed [μm s <sup>-1</sup> ]	570	800	980	1130	1260	1390

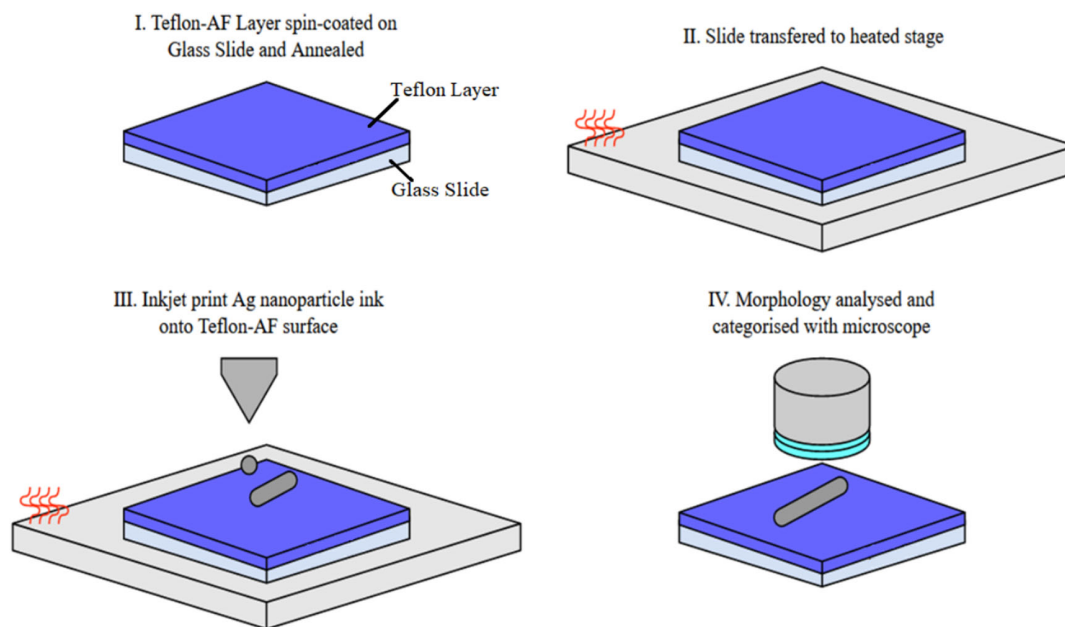


**Figure 2.** Schematic diagram of experimental method.

wettability gradients experienced by impacting overlapping droplets result in negligible droplet shifts, allowing for a maximized range of printability conditions. While wet droplets are still affected by the wettability gradient, complete overlap onto the previous droplet is not achieved before drying. This results in an offset of the droplet to be sintered on the substrate surface. This can be seen by the repeatability of enlarged groups of droplets and their spacings remaining consistent (Figure 3b). This predictability in the size of droplet groups indicates the specific shift of each droplet in a grouping until intrinsic group separation occurs. The predictably regular spacings and sizes of the groupings indicates that droplet behavior is predictable and is not subject to small fluctuations or errors in printing conditions. Therefore, this is identified as a separate regime from isolated droplets. The onset of this condition is heavily dependent on droplet spacing, substrate temperature, and stage speed/deposition frequency. Because of this, grouping behavior does not have a singular observed maximum length before transitioning into the next regime.

The broken line regime (Figure 3c) exists as a transitional regime between isolated multi-droplets and true stacked coin morphology (Figure 3d). Droplet groupings begin displaying unpredictable behavior, with groupings of unstable lengths beginning to occur at various intervals. Within this regime, full stacked coin lines up to 1000  $\mu\text{m}$  can be produced, however, when repeating the test conditions, a different pattern of grouping segments is observed. This morphology can exist within conditions where the overlap, drying time, and deposition rate are sensitive to experimental conditions which can cause a line breakage, thus these regions are not identified as printable regions for true stacked coin morphology. The presence of this regime can indicate onset conditions of the stacked coin regime. This regime tends to occur more frequently at large drop spacings due to poor droplet pinning upon impact. This can

be used to identify the minimum overlap limit and speed limit for printing success.

The true stacked coin regime indicates printing conditions that yield continuous lines adhering to stacked coin morphology (Figure 3d). This is the ideal printing regime, and this study aims to discover the conditions necessary for a variety of speeds, drop spacings, and substrate temperatures for which stack coin regimes can be observed. We want to achieve situations where stacked coins can be produced at the lowest possible temperature, with the highest stage speed, and the lowest volume of droplets used.

There is yet another regime observed, which takes place under narrow conditions when drop and stage speed is low, while stage temperature is high (Figure 3e). Delamination refers to printed lines partially lifting from the surface. This partial delamination is the result of tensile forces across the printed line; the tail of the delaminated line begins to rise off the surface. Full delamination has also been observed. While partial delamination has been observed to self-limit, full delamination has not been observed to stop once it has started. A similar phenomenon with the curling up of inkjet-printed lines has been observed and utilized previously,<sup>[30]</sup> with the root cause being a product of the built-up stress gradient within the silver nanoparticle ink due to the rapid drying and high stage temperature experienced by the lines. The delamination of the line is a result of the low adhesion of the Teflon-AF to the glass slide, as seen by the imprints left on the substrate due to a ripped Teflon-AF layer (Figure 3e-i,ii). The imprints left on the substrate show the detachment of the Teflon-AF layer from the surface of the glass slide. Thus, despite the initial poor adhesion of silver to the Teflon, it is greater than that of the Teflon to the glass. The presence of the delamination phenomenon indicates a regime where true stacked coin lines cannot be reliably produced. The variant of delamination can be identified within the imprint left on the Teflon-AF surface

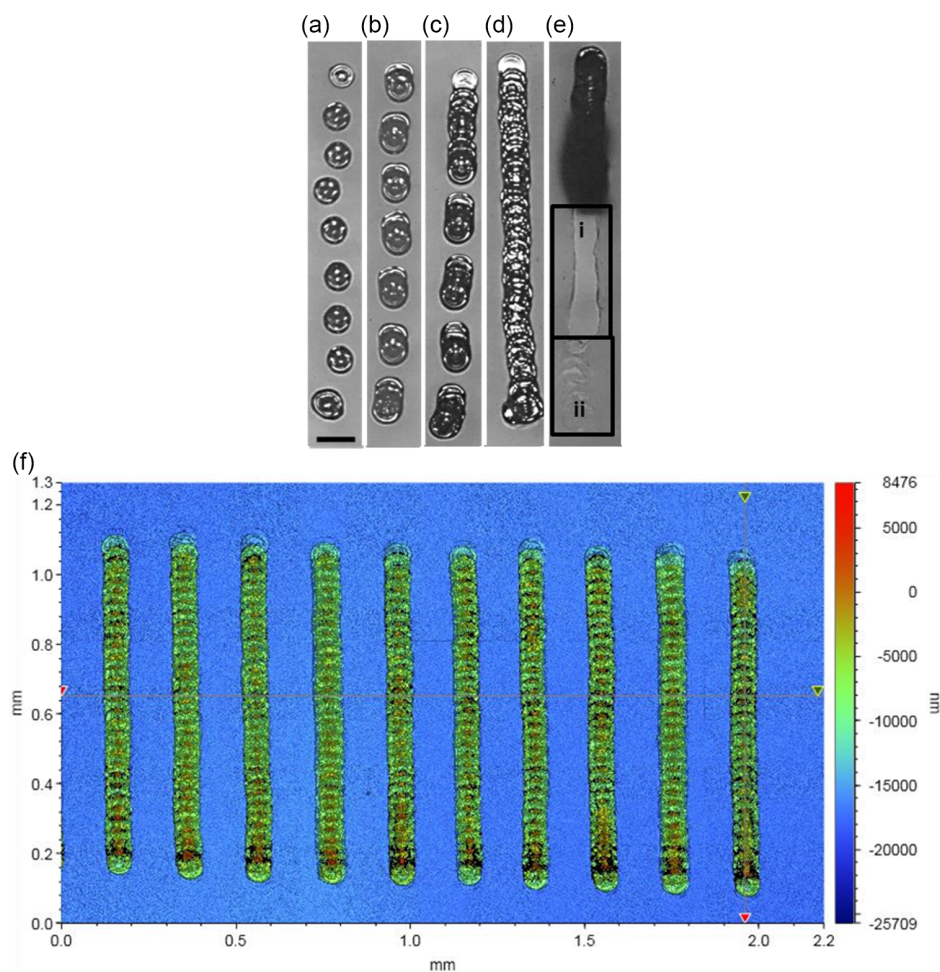


**Figure 3.** Identified line printing regimes: a) isolated droplets, b) isolated multi-droplets, c) broken lines, d) true stacked coin, and e) delamination regime—i) partial delamination and ii) full delamination with differing patterns on Teflon-AF. Scale bar 100  $\mu\text{m}$ . f) Optical profilometry example with a group of 10  $\mu\text{m}$  drop spacing true stacked coin lines.

as seen in (Figure 3e—see boxes labeled “i” and “ii”) below with full delamination stripping all the coated Teflon-AF from the glass substrate while the initial partial delamination region shows only removal of the Teflon-AF at the points of highest surface adhesion. The key characteristics and necessary printing conditions of each regime are unique and summarized in Table 2. The data points in Figure 4 show the parameters

experimentally investigated within this study, while the space between these points reflects the respective regimes of the surrounding points.

Figure 4 shows regime maps for various experimental conditions. The regime maps displayed clearly show that ink behavior can be controlled by the stage movement speed, substrate temperature, and droplet spacing. The regime maps indicate that the

**Table 2.** Summary of identified regime specifications and necessary printing conditions.

Regimes	Stage temperature [ $^{\circ}\text{C}$ ]	Stage speed [ $\mu\text{m s}^{-1}$ ]	Drop spacing [ $\mu\text{m}$ ]	Notes
Isolated droplets		Common morphology for ink printed on hydrophobic surfaces without surface temperature control.		
Isolated multi-droplets	150–180	Dependent on temperature and drop spacing	5–30	Predictable.
Broken line	>150		5–30	Poor droplet pinning, unpredictable.
True stacked coin	>150		<25	Predictable, topology dependent temperature and stage speed.
Delamination	175–180	<10	<10	Poor surface pinning, unpredictable.

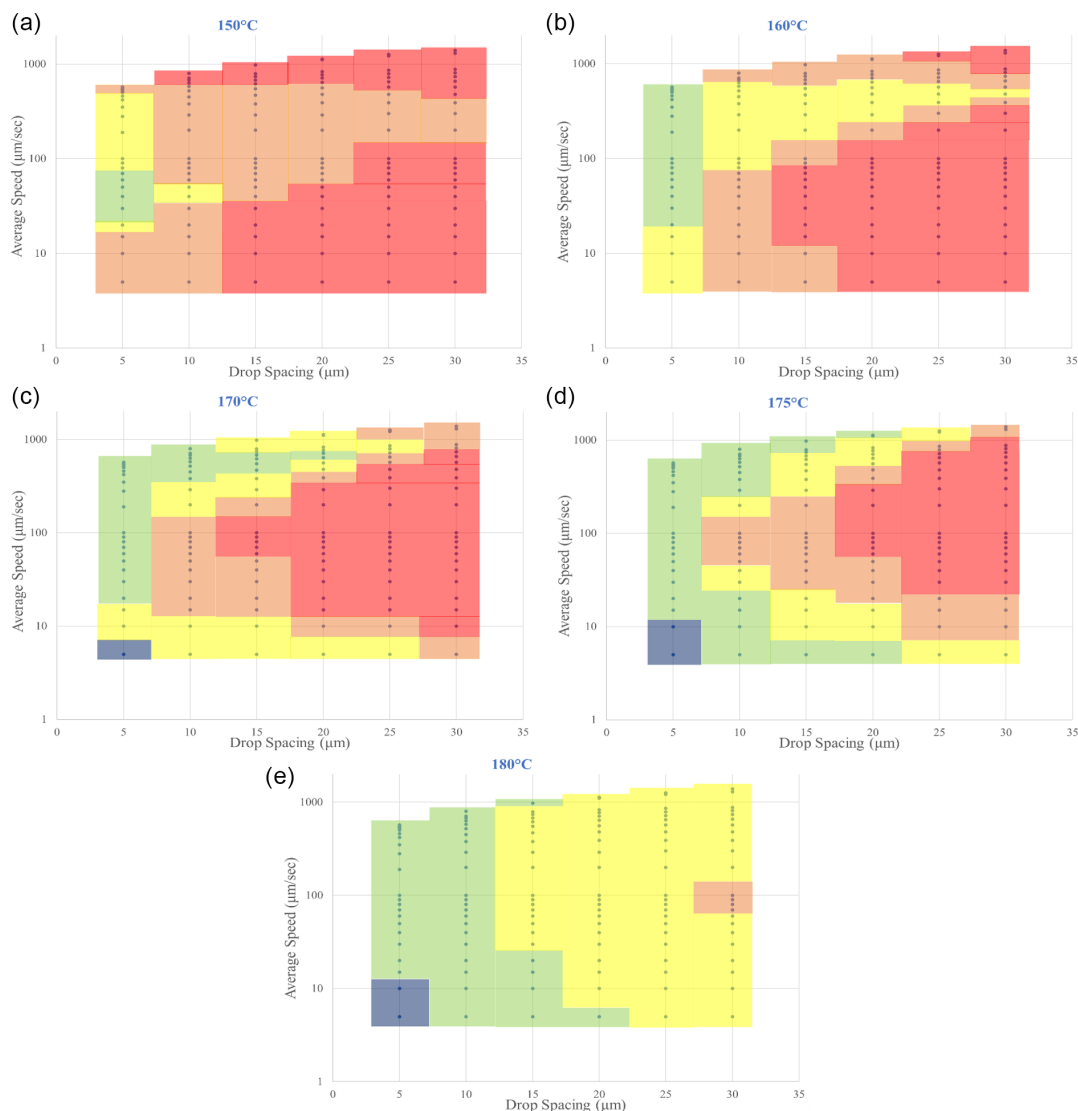


**Figure 4.** Printing regime maps for printed line morphologies on hydrophobic substrate at a) 150 °C, b) 160 °C, c) 170 °C, d) 175 °C, and e) 180 °C.

success of this technique favors regions of high droplet overlap, and high substrate temperature. Additionally, the maps shows clear cooperative trends between all three of the controlled variables in improving line printability. The overlapping droplets are subject to lower contact angles in overlapped regions, which positively influences the printability of low drop spacings due to the pinning of ink on dried droplets. Also, at lower contact angles, it is observed that ink dries faster than their counterparts with larger contact angles.<sup>[31]</sup> The effect of increasing droplet overlap (or decreasing the drop spacing) is reflected in the regime maps, with systems printed with higher droplet overlap experiencing a larger range of conditions resulting in true stacked coin line formation (recall dried droplets are hydrophilic). This suggests that increasing droplet volume could briefly improve printability before the effects of stage temperature begin to decline. As drop spacing is increased, the range of stacked coin formation decreases until reaching the system limits (Figure 4a–e),

e.g., drop spacing of 20 and 25  $\mu\text{m}$  for substrate temperature of 170 °C or higher.

The critical temperature of the system is defined as the temperature where only lines exhibiting true stacked coin or broken stacked coin behavior are recorded. This was found to be 180 °C. This temperature can be further identified through observing the changing morphologies of true stacked coin lines as we approach this temperature as seen in **Figure 5**. It is expected that increasing the hydrophobicity of the system would increase the critical temperature of the system, as drying times and the strength of dewetting of droplets are influenced by droplet contact angle.<sup>[31]</sup>

At lower temperatures, it is clear from the drying patterns that temperature is influential in the final morphologies of each regime. This is evidenced by the chaotic drying patterns at lower temperatures transitioning into a predictable stacked coin morphology at higher temperatures (Figure 4a–d). Droplet coalescence is significantly influenced by spreading while sintering.

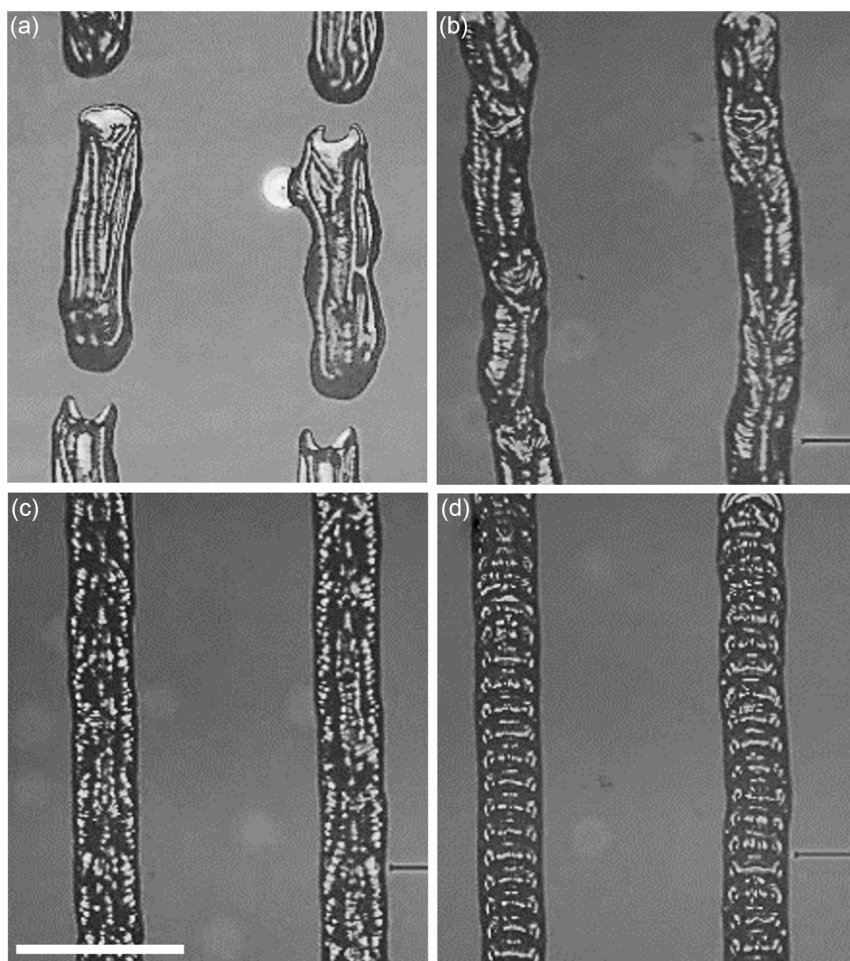


**Figure 5.** Comparison of 10  $\mu\text{m}$  drop spacing lines exhibiting enhanced droplet coalescence during sintering due to spreading: a) temperature 160  $^{\circ}\text{C}$ ; b) temperature 170  $^{\circ}\text{C}$ ; c) temperature 175  $^{\circ}\text{C}$ ; and d) instantaneous drying characteristic morphology temperature 180  $^{\circ}\text{C}$ ; all at average stage speed 800  $\mu\text{m}\cdot\text{s}^{-1}$ ; white scale bar—200  $\mu\text{m}$ .

As the system approaches the temperature of instantaneous drying, line morphologies begin to exhibit less evidence of wet droplet coalescence dynamics. At high temperatures, impacting droplets can produce individual coffee ring structures or raised rims when drying on a pre-dried droplet. The coffee ring effect is a well-known phenomenon leaving a ring-like deposit of particles upon the contact line of a colloidal solution, e.g., silver nanoparticle ink. The coffee ring effect is due to droplet evaporation at the liquid–gas interface of the droplet promoting mass flux to the droplet edges, leading to particle build up at the droplet contact line.<sup>[32]</sup> The coffee ring effect is enhanced at high temperatures, thus being an indicator that the instantaneous drying condition is prevailing,<sup>[3]</sup> see the structure of lines created in Figure 5d.

The effect of any controllable variable is largely dependent on the other two, with stage speed, stage temperature, and droplet spacing all affecting the influence of one another on achieving stacked coin printing. At temperatures above 170  $^{\circ}\text{C}$ , an increasing stage speed initially trends regime transitions toward isolated droplets. However, as stage speed continues to increase line printability begins to improve, trending regime transitions

toward true stacked coin. While at lower temperatures (150–170  $^{\circ}\text{C}$ ), there appears to be distinct speed ranges where printability will improve before deteriorating again. This key difference in ink behavior indicates the onset of the critical temperature, as lower temperatures possess considerable influence from droplet coalescence dynamics. Upon further increasing the stage speed, line printability begins to improve across all substrate temperatures and drop spacings. The difference in increasing stage speed behaviors between the two speed ranges is a result of the asymmetric droplet impact spreading due to the stage movement at higher speeds (Figure 7). Asymmetric droplet impact spreading occurs when droplets impact a stage with sufficiently high speed to promote deformation and asymmetric spreading.<sup>[33]</sup> Typically, inkjet printing electronics are printed at speeds in the order of 10–100  $\text{mm}\cdot\text{s}^{-1}$ , which is significantly faster than stage speeds within this article.<sup>[34]</sup> This is due to the limitations of the DOD vector printing apparatus having a maximum speed of around 1000  $\mu\text{m}\cdot\text{s}^{-1}$  for the small drop spacing necessary to achieve stacked coin printing on hydrophobic substrates.

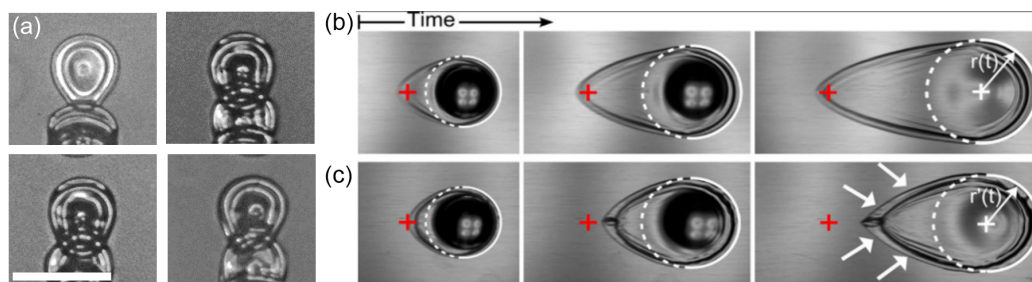


**Figure 6.** a) Dried droplet spreading behaviour at system critical temperature ( $25\ \mu\text{m}$  drop spacing at elevated stage speed with identical printing conditions), white scale bar— $100\ \mu\text{m}$ ; asymmetric droplet spreading due to induced stage movement during impact on b) hydrophilic surface. Reproduced with permission.<sup>[33]</sup> c) Hydrophobic surface with Lagrangian frame of reference, reproduced with permission<sup>[33]</sup>; “+” on (b) and (c) signifies the initial impact point of droplet.

**Figure 6** highlights the similarities between the structure of dried droplets at high stage speeds and temperatures, and the observed asymmetric spreading of an impacting droplet on a moving stage. At high stage speeds, asymmetric droplet morphology is observed over all overlapping droplets which comprise a connected chain (**Figure 7**).

Figure 7 shows consistent asymmetric droplet spreading across lines of  $30\ \mu\text{m}$  drop spacing at elevated stage speed conditions, with droplets of all drop spacings showing the same spreading behavior when printed at these speeds. Upon further inspection, only droplets which have observable overlap to the previous droplet in the system express an asymmetric droplet profile. This means that while droplets will be subject to asymmetric deformation due to the high stage speeds, they will only retain this beneficial shape if drops have experienced sufficient contact line pinning to the previous droplet in the system. Droplets with a circular profile in Figure 6 are situated at the beginning of a multi-droplet group, indicating that due to a combination of poor pinning to the previous droplet and the high receding contact angle may have caused this droplet to depin from the previous drop resulting in a breakage. The circular droplet structures (seen in Figure 7) are a result of the retraction of the tail of the droplets on hydrophobic surfaces due to the poor surface adhesion (Figure 6b,c). Having attempted to replicate the asymmetric droplet spreading profile on singular, non-overlapping droplets, only purely circular droplet splats were observed. This demonstrated the mechanisms of line formation

that depends on droplet pinning for successful deformation patterns.

Almohammadi et al.<sup>[33]</sup> have previously investigated the dynamics and profiles of impacting droplets onto moving substrates, for both hydrophobic and hydrophilic surfaces. Their work provides a comprehensive examination of droplet lamella growth across a range of surfaces and droplets and is reflected again in the samples and results we have reported in this work. Despite the conditions of droplet impact and experimental setup being different, there exists correlation between the droplet spreading images they have taken and the dried droplet profiles seen when using this technique at high stage speeds, Figure 5 and 6. The occurrence of this unique droplet profile within our experimental images also reflects an increase in printability seen at high stage speeds, e.g., in Figure 4c,d. The asymmetric spreading of drops increases the length of droplets as they impact and sinter upon the surface, which can result in larger droplet overlap conditions being satisfied with subsequent overlapping droplets. With a large overlap onto the hydrophilic surface of the dried droplet, subsequent droplets can more efficiently sinter and pin to the surface, thus increasing the printability at higher speeds. At lower temperatures, it is clear from the drying patterns that this effect is influential in the dried droplet profile, seen by the unpredictable and chaotic drying patterns seen for lines, Figure 5. The onset of advantageous changes in droplet regimes due to stage speed conditions occurs from  $100$  to  $200\ \mu\text{m}\ \text{s}^{-1}$ , the investigation into stage speed is limited

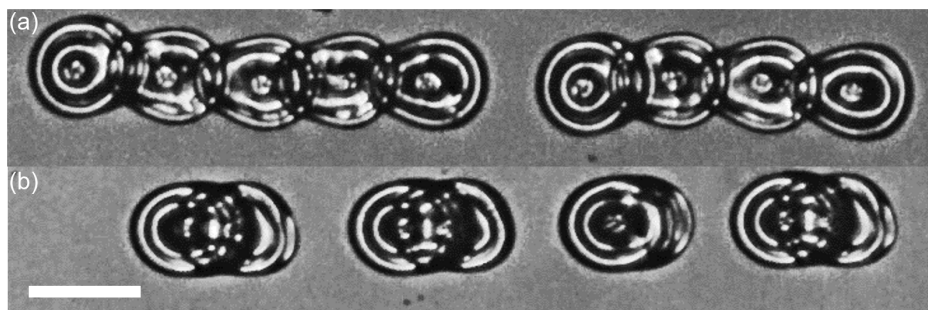


**Figure 7.** Difference in average grouping size resulting from dried droplet spreading behaviour at system critical temperature ( $180\ ^\circ\text{C}$ ): a)  $30\ \mu\text{m}$  spacing approaching maximum speed with asymmetric droplet spreading (broken line regime), b)  $30\ \mu\text{m}$  spacing at  $100\ \mu\text{m}\ \text{s}^{-1}$  without asymmetric droplet spreading (isolated multi-droplet regime). White scale bar— $100\ \mu\text{m}$ .

by the acceleration capabilities of the setup. The limitations of droplet spreading is an important point of further research to identify the limitations of the throughput of this technique. Despite this, the spreading mechanisms observed at high temperatures positively influence printability and this is expected to remain true for higher speeds.

In addition to the successful and reliable printing of connecting lines on hydrophobic substrates, the true stacked coin printing regime can also be used to construct patterns (e.g., squares) on hydrophobic substrates (**Figure 8**). The success of this technique in printing 2D structures improves the viability in applications within the field of printed electronics. We found that in the determination of resistivity of our structures without post curing, the printed square shape was a more reliable structure for determining sheet resistance and thickness. The resistivity was calculated through multiplying sheet resistance by thickness. The sheet resistance of the printed square was calculated using van der Pauw by placing the measuring probes at the four corners of the square.<sup>[35]</sup> The thickness of the square was extracted from the confocal microscopy data and was averaged over the entire square (26  $\mu\text{m}$ ) finding the resistivity to be  $2.40 \times 10^{-6} \Omega \text{ cm}$ . This measurement is in line with standard resistivity of silver nanoparticle inks of about 3–16  $\Omega \text{ cm}$ ,<sup>[36]</sup> further highlighting the capability of this technique. Due to the drying of the ink droplets being intrinsic to the success of this technique, there was no need for ink postcuring after printing. This technique has demonstrated both successes in conductivity and the additional benefit of incorporating the curing step into the printing process.

The proposed method for printing is successful, but there are some drawbacks as well. The first being the technical issue

of nozzle clogging. During the production of lines, it is not uncommon for ink entrained within the nozzle to sinter due to radiative heat from the stage. The closer the printhead to the stage, the more exposed it is to radiative heat and thus is more susceptible to nozzle clogging. Nozzle clogging is more prevalent at lower stage speeds due to the increased time between droplet jetting allowing the nozzle tip to be further influenced by the stage temperature. In addition to nozzle clogging, printed lines experience low mechanical resistance. Printed lines have been observed breaking upon contact with probes during electrical measurements, a factor furthermore influenced by both the low adhesion of Teflon to the glass slide and the silver to the Teflon.

It is currently unclear how this technique would behave at higher speeds, regime maps at lower stage speeds (**Figure 4a,b**) show that regimes begin to transition toward isolated droplets after previously experiencing transitions toward true stacked coin. This is not reflected at higher stage temperatures within the observed limits of the experimental system. Higher stage speeds would further impact line formation phenomena as there may be a limit to the enhanced printability caused by asymmetric spreading. While this study has utilized stage heating to achieve a fast-drying condition, this limits the application of the technique to substrates which are not thermosensitive relative to the instantaneous drying temperature of the ink. Despite this, the intrinsic mechanisms of the developed technique can be applied to ultraviolet (UV) sensitive conductive ink options, overcoming the thermosensitivities of a substrate while ensuring instantaneous drying with UV radiation. The timescale of droplet ejection versus evaporation is a key factor for consideration within this technique.

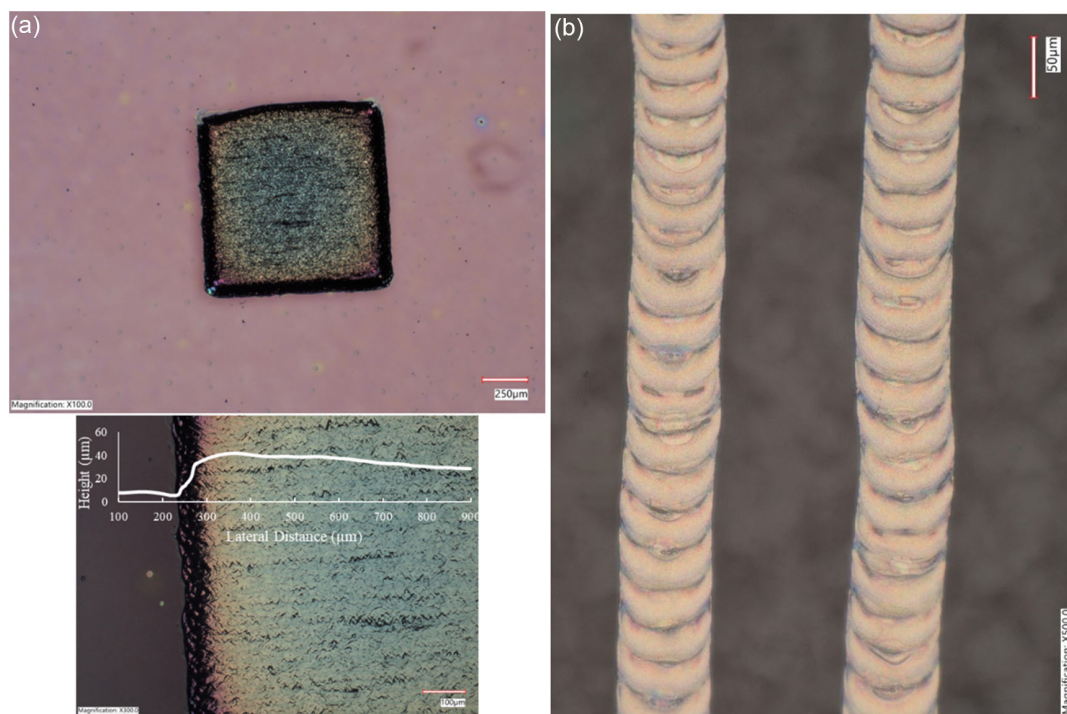


**Figure 8.** a) Square structure on hydrophobic substrate achieved through application of stacked coin printing, 180  $^{\circ}\text{C}$ , 800  $\mu\text{m s}^{-1}$ , 10  $\mu\text{m}$  drop spacing. b) Close-up of connecting silver lines in true stacked coin regime.

## 4. Conclusions

In conclusion, we have developed a method of inkjet printing conductive ink onto hydrophobic substrates without the use of expensive, time-consuming, or complicated pretreatment processes. The effects of stage speed, droplet spacing, and stage temperature have been identified as the key working parameters controlling line printability. Five distinct printability regimes (isolated droplets, isolated multi-droplets, broken line, true stacked coin, and delamination) have been identified which map out regions of printability across the key printable parameters. The mapping of printability regimes based on temperature and drop spacing can thus be used to successfully predict the onset conditions of true stacked coin morphology. Regime maps have been developed with respect to each of the identified key printing parameters, successfully highlighting the trends, which can be used to predict regime transitions. The critical temperature of the system, ensuring instantaneous drying at all applicable drop spacings was found to be 180 °C. A maximum drop spacing of 20 μm was identified, above which successful printing of the true stacked coin regime is unachievable. The stage speeds found to be the most successful in printing successful lines vary depending on the drop spacings, however, the maximum stage speeds achieved for drop spacings of 5–15 μm are recommended for future use (570–980 μm s<sup>-1</sup>, respectively). The influence and effect of the asymmetric spreading phenomenon, occurring at high stage speeds, shows distinct promise for scale-up potential and for the use of higher stage speeds in future. The stage speed was found to affect the system differently depending on droplet drying time, however, speeds up to 20 μm s<sup>-1</sup> are the most sensitive to rapid regime changes. Additionally, asymmetric droplet spreading has been identified as a key phenomenon, which improves the printability of these lines showing distinct promise for achieving higher line throughputs in the future.

## Supporting Information

Supporting Information is available from the Wiley Online Library or from the author.

## Acknowledgements

The authors would like to gratefully acknowledge the financial support received from the ThermoSMART project of the European Commission (grant: EC-H2020-RISE-ThermoSMART-778104) and the Natural Sciences and Engineering Research Council of Canada (NSERC), funding reference number STPGP 521480-18. For the purpose of open access, the author has applied a Creative Commons Attribution (CC BY) licence to any Author Accepted Manuscript version arising from this submission.

## Conflict of Interest

The authors declare no conflict of interest.

## Data Availability Statement

The data that support the findings of this study are available from the corresponding author upon reasonable request.

## Keywords

stacked coin, conductive ink, droplet, hydrophobic surface, inkjet printing

Received: January 29, 2024

Revised: March 20, 2024

Published online:

- [1] W. Wu, *Nanoscale* **2017**, *9*, 7342.
- [2] Y. Lin, Y. Gao, Z. Fan, *Adv. Mater.* **2017**, *29*, 1701736.
- [3] D. Soltman, V. Subramanian, *Langmuir* **2008**, *24*, 2224.
- [4] S.-H. Lee, K.-Y. Shin, J. Y. Hwang, K. T. Kang, H. S. Kang, *J. Micromech. Microeng.* **2008**, *18*, 075014.
- [5] P. Naderi, G. Grau, *Org. Electron.* **2022**, *108*, 106612.
- [6] P. Naderi, B. R. Sheuten, A. Amirfazli, G. Grau, *J. Chem. Phys.* **2023**, *159*, 024712.
- [7] C. Liu, R. D. Arnell, A. R. Gibbons, S. M. Green, L. Ren, J. Tong, *Surf. Eng.* **2000**, *16*, 215.
- [8] M. Trotter, D. Juric, Z. Bagherian, N. Borst, K. Gläser, T. Meissner, F. von Stetten, A. Zimmermann, *Sensors* **2020**, *20*, 1333.
- [9] S.-H. Lee, Y. Xu, D. Khim, W.-T. Park, D.-Y. Kim, Y.-Y. Noh, *ACS Appl. Mater. Interfaces* **2016**, *8*, 32421.
- [10] K. Fukuda, Y. Takeda, Y. Kobayashi, M. Shimizu, T. Sekine, D. Kumaki, M. Kurihara, M. Sakamoto, S. Tokito, *Jpn. J. Appl. Phys.* **2013**, *52*, 05DB05.
- [11] T. Sekine, H. Ikeda, A. Kosakai, K. Fukuda, D. Kumaki, S. Tokito, *Appl. Surf. Sci.* **2014**, *294*, 20.
- [12] J. Lefebvre, J. Ding, Z. Li, F. Cheng, N. Du, P. R. L. Malenfant, *Appl. Phys. Lett.* **2015**, *107*, 243301.
- [13] W. C. Shin, S. Seo, B. J. Cho, *Appl. Phys. Lett.* **2011**, *98*, 153505.
- [14] J.-S. Kwon, D. Lee, J. Oh, *Appl. Sci.* **2018**, *8*, 280.
- [15] D. Astaneh, R. Burlica, D.-E. Cretu, M. Olariu, I. Stoica, O. Beniuga, *Materials* **2022**, *15*, 1919.
- [16] D. Tian, Y. Song, L. Jiang, *Chem. Soc. Rev.* **2013**, *42*, 5184.
- [17] H. Y. Park, B. J. Kang, D. Lee, J. H. Oh, *Thin Solid Films* **2013**, *546*, 162.
- [18] R. Abunahla, M. S. Rahman, P. Naderi, G. Grau, *J. Micro Nano-Manuf.* **2020**, *8*, 031001.
- [19] J. Godleman, F. Leroux, S. Reynolds, J. Philpott, P. B. Cranwell, J. L. Harries, W. Hayes, H. M. Colquhoun, *Prog. Org. Coat.* **2021**, *158*, 106378.
- [20] S. Kim, H. W. Kang, K. H. Lee, H. J. Sung, *J. Micromech. Microeng.* **2011**, *21*, 095026.
- [21] J. Sung, B. J. Kang, J. H. Oh, *Microelectron. Eng.* **2013**, *110*, 219.
- [22] J. Kwon, S. Baek, Y. Lee, S. Tokito, S. Jung, *Langmuir* **2021**, *37*, 10692.
- [23] A. Shimoni, S. Azoubel, S. Magdassi, *Nanoscale* **2014**, *6*, 11084.
- [24] Y. Kim, B. Lee, S. Yang, I. Byun, I. Jeong, S. M. Cho, *Curr. Appl. Phys.* **2012**, *12*, 473.
- [25] V. Grishae, C. S. Iorio, F. Dubois, A. Amirfazli, *J. Colloid Interface Sci.* **2017**, *490*, 108.
- [26] C. Antonini, A. Amirfazli, M. Marengo, *Phys. Fluids* **2012**, *24*, 102104.
- [27] Y. F. Liu, M. H. Tsai, Y. F. Pai, W. S. Hwang, *Appl. Phys. A: Mater. Sci. Process.* **2013**, *111*, 509.
- [28] B. Derby, *Annu. Rev. Mater. Res.* **2010**, *40*, 395.
- [29] Y. Xiang, P. Fulmek, D. Platz, U. Schmid, *Langmuir* **2022**, *38*, 1631.
- [30] M. A. Karim, T. Lee, E. Alon, V. Subramanian, *Adv. Electron. Mater.* **2016**, *2*, 1500482.
- [31] S. Chandra, M. di Marzo, Y. M. Qiao, P. Tartarini, *Fire Safety J.* **1996**, *27*, 141.
- [32] R. D. Deegan, O. Bakajin, T. F. Dupont, G. Huber, S. R. Nagel, T. A. Witten, *Nature* **1997**, *389*, 827.

- [33] H. Almohammadi, A. Amirfazli, *Langmuir* **2017**, *33*, 5957.
- [34] H. Al-Chami, E. Cretu, in *2009 IEEE 15th Inter. Mixed-Signals, Sensors, and Systems Test Workshop*, Scottsdale, AZ, USA, **2009**, pp. 1–6, <https://doi.org/10.1109/ims3tw.2009.5158692>.
- [35] M. Ghalamboran, M. Nazari, G. Grau, *Flex. Print. Electron.* **2024**, *9*, 015011.
- [36] A. Chiolerio, K. Rajan, I. Roppolo, A. Chiappone, S. Bocchini, D. Perrone, *Nanotechnol. Sci. Appl.* **2016**, *2016*, 1.